https://ntrs.nasa.gov/search.jsp?R=19820004822 2020-03-21T11:37:34+00:00Z

View metadata, citation and similar papers at core.ac.uk

brought to you by CORE

provided by NASA Technical Reports Serve

N O T I C E

THIS DOCUMENT HAS BEEN REPRODUCED FROM MICROFICHE. ALTHOUGH IT IS RECOGNIZED THAT CERTAIN PORTIONS ARE ILLEGIBLE, IT IS BEING RELEASED IN THE INTEREST OF MAKING AVAILABLE AS MUCH INFORMATION AS POSSIBLE

NSG-7610

GLOBAL ISOTATIC GEOID ANOMALIES FOR PLATE AND BOUNDARY LAYER MODELS OF THE LITHOSPHERE

Bradford H. Hager

Seismology Laboratory
Division of Geological and Planetary Sciences
California Institute of Technology
Pasadena, California 91125

(NASA-CR-164985) GLOBAL ISOSTATIC GEOID ANOMALIES FOR PLATE AND BOUNDARY LAYER MODELS OF THE LITHOSPHERE (California Inst. of Tech.) 34 p HC A03/MF A01 CSCL 08G

N82-12695

Unclas
G3/46 08328

November 10, 1981

Abstract

Commonly used one-dimensional geoid models predict that the isostatic geoid anomaly over old ocean basins for the boundary-layer thermal model of the lithosphere is a factor of two greater than that for the plate model. Calculations presented here, using the spherical analogues of the plate and boundary-layer thermal models, show that for the actual global distribution of plate ages, one-dimensional models are not accurate and a spherical, fully three-dimensional treatment is necessary. The maximum difference in geoid heights predicted for the two models is only about two meters. The thermal structure of old lithosphere is unlikely to be resolvable using global geoid anomalies. Stripping the effects of plate aging and a hypothetical uniform, 35 km, isostatically-compensated continental crust from the observed geoid emphasizes that the largest-amplitude geoid anomaly is the geoid low of almost 120 m over West Antarctica, a factor of two greater than the low of 60 m over Ceylon.

1. Introduction

One of the more striking successes of the kinematic model of plate tectonics is that the variation in oceanic depth away from ridges can be understood in terms of simple models of cooling of the lithosphere (1-5). Oceanic heat flow can be explained by these models if hydrothermal activity at the ridge is taken into account (6); recently it has been demonstrated that the short wavelength change in geoid elevation over ridges predicted by these simple models is also readily observed (7-9).

A number of models have been proposed for the thermal evolution of the lithosphere. In the boundary layer model, the uppermost mantle is supposed to cool by conduction, with the lithospheric thickness increasing as the square root of age (2,5). In the plate model, the temperature is assumed to be held fixed by some mechanism at a depth on the order of 100 km (1,3,4). The models are quite similar near the ridge crest before cooling has penetrated very deep, but over the ocean basins, the models differ substantially.

Other thermal models have been proposed which include the effects of latent heat from freezing partial melts (10), pressure gradients from return flow (11,12), heat flux into the base of the lithosphere (13), and heat sources at the base of or below the lithosphere (14,15). Any or all of these effects may be important in the earth, but in this paper, discussion will be focused primarily on the differences between the plate and boundary layer models.

Three types of observations have been proposed to provide possible constraints on the thermal structure of the lithosphere. Heat

flow is proportional to the surface temperature gradient. The surface temperature gradients for the plate and boundary layer models differ only slightly for lithosphere less than 200 Myr old, however, so heat flow is not at present useful for distinguishing between these models (16).

Seafloor elevation is related to the average heat content of the underlying column of rock. As the uppermost mantle cools while moving away from the ridge, it contracts, leading to an increase in ocean depth. The total increase in ocean depth with time (assuming constant thermal expansivity) is proportional to the change in the average heat content of that part of the mantle which is dynamically coupled to the surface, not, in general, the lithosphere alone (15). This change in heat content is just the difference between the time-integrated heat flux out the system and any internal heating or flux of heat into the system. The standard boundary layer and plate models (assuming dynamic decoupling at the base of the plate) predict different seafloor elevations for old lithosphere; although the heat flow out of each is nearly identical, the plate model supposes that extra heat is added to the system at the base of the plate. This specifically-located heat source would be indistinguishable from any more general distribution of internal heat sources, however, since topography gives only a measure of the average heat content.

A third potentially useful observation is geoid height. In the one-dimensional (long wavelength) limit, the geoid height is proportional to the first moment of the density distribution (7-9). Because it is sensitive to the distribution of density, geoid height in

principle might be expected to provide a more sensitive constraint on thermal models than heat flow or seafloor topography, which depend upon surface gradient and average heat content respectively.

In the one-dimensional limit, the geoid heights for the two models discussed here differ by a factor of two over old ocean basins (17). The actual distribution of lithospheric ages is distinctly three-dimensional, however, so the validity of the one-dimensional calculation is not a priori guaranteed. Model geoids computed using an estimate of the actual distribution of seafloor ages are presented below. Unfortunately, the full three-dimensional, spherical calculation shows that the difference between the geoids computed for the two lithosperic models is very small and unlikely to be observable.

2. Calculation of Isostatic Geoid Anomalies

Dahlen (18) has recently discussed the application of the concept of isostacy to a sphere, noting that the theoretical geoid anomaly is very sensitive to the exact definition used for isostacy. Isostatic geoid anomalies are by nature first order quantities; if they are to be computed to first order, isostacy must be defined to second order. Dahlen showed that geoid anomalies could differ by more than a factor of two, depending on the definition chosen, e.g., constant pressure at the level of compensation versus constant mass above the level of compensation.

In this paper, the isostatic condition is assumed to correspond to a local compensation such as would be achieved by a set of vertical (or conical) piles of different lengths and densities decoupled

from each other floating in an inviscid fluid. The weight of any pile is taken to be equal to the weight of fluid displaced by the pile. Self-compression in the earth causes the gravitational acceleration g to be essentially constant with depth, so the constant weight criterion is equivalent to a constant mass criterion. For a halfspace, isostacy is achieved if

$$\int \Delta\rho \, dz = 0 \tag{1}$$

where z is depth, and $\Delta\rho$ is the density contrast between the pile and the fluid. The integral is taken over the depth of the pile, i.e., the region in which density contrasts are nonzero, which, in this paper, corresponds to the thickness of the lithosphere, h.

For a sphere, the equivalent definition is that

$$\int \Delta\rho \left(\frac{a - z}{a}\right)^2 dz = 0 \tag{2}$$

where a is the radius of the earth. Since $h \ll a$ and $\Delta\rho$ is a first order quantity, (1) and (2) are equivalent to first order, but they result in different gravitational potential anomalies (18).

In calculating the geoid anomaly from an arbitrary density distribution, it is convenient to separate the horizontal and depth dependences of density. The horizontal dependence is expressed in terms of harmonic functions. For a flat earth, the contribution of density contrasts $\Delta\rho_k(z)$, of wavelength k, extending over depth h, to the geoid height, $N_k(\chi)$, can be written:

$$N_k(\underset{\sim}{x}) = \frac{2\pi G}{g} e^{i(\underset{\sim}{k}\cdot\underset{\sim}{x} + \phi_k)} \int \Delta\rho_k(z) e^{-kz} dz \qquad (3)$$

Here $\underset{\sim}{x}$ is the horizontal position vector, G the gravitational constant, g the gravitational acceleration, and ϕ_k a phase angle.

Taking (1) as the definition of isostacy and assuming $kh \ll 1$ leads to the simplification

$$N_k(\underset{\sim}{x}) = \frac{-2\pi G}{g} e^{i(k\cdot x + \phi_k)} \int z\Delta\rho_k dz \qquad (4)$$

This approximation is in error by less than 10% for $kd < .2$, or for wavelengths greater than 3800. km if h corresponds to the plate thickness of 120 km. It overestimates the geoid height contribution from shorter wavelengths.

For a sphere, horizontal density contrasts can be expressed in terms of surface spherical harmonics $Y_{\ell m}(\theta,\phi)$ of degree ℓ and order m. The equivalent of (3) is then

$$N'_{\ell m}(\theta,\phi) = \frac{4\pi G a}{g(2\ell + 1)} Y_{\ell m}(\theta,\phi) \int \Delta\rho_{\ell m}(z) \left(\frac{a-z}{a}\right)^{\ell+2} dz \qquad (5)$$

where a is the radius of the earth. For h/a << 1, using (2) leads to

$$N'_{\ell m}(\theta,\phi) = \frac{-4\pi G}{g} \frac{\ell}{2\ell + 1} Y_{\ell m}(\theta,\phi) \int z\Delta\rho_{\ell m}(z)dz \qquad (6)$$

In this case, the approximation is in error by less than 10% for $\ell < 12$ if h = 120 km. For $\ell = 20$, (6) overestimates the contribution of a density contrast at a depth of 120 km by 20%.

An additional complication arises for isostatic compensation on a spherical earth. The interior of the earth is assumed to be inviscid on the timescales applicable to isostatic equilibrium. The gravitational potential from an isostatically compensated mass will cause a net deformation of the (fluid) earth. This deformation, in turn, causes an additional gravitational potential, which leads to yet more deformation.

This is a classical problem in geophysics which has often been solved for the degree two deformation associated with earth rotation and tides using Love numbers (19). The total geoid anomaly $N_{\ell m}$ is given by

$$N_{\ell m} = H_\ell N'_{\ell m} \qquad (7)$$

where H_ℓ is the Love number for degree ℓ.

Exact computation of the Love numbers for a fluid sphere which has the density and compressibility distribution of the earth is a formidable task. To my knowledge, it has been done only for degree two,

for which $H_2 = 1.96$ (19). The effect of interior density contrasts is to increase H_ℓ, as deformation of internal boundaries supplements the perturbing potential. Compressibility decreases H_ℓ.

Rather than solve for each Love number using a realistic earth model, I have chosen to use an approximate model calibrated using the known value of H_2. The earth is assumed to be a sphere of incompressible fluid of density ρ with a point mass at the center sufficient to bring the average density of the sphere to $\bar{\rho}$. The Love number H_ℓ for such a system is given by:

$$H_\ell = \frac{2\ell+1}{2\ell+1 - 3\rho/\bar{\rho}} \quad , \tag{8}$$

which reduces to $(\ell + 1/2)/(\ell - 1)$ for $\rho = \bar{\rho}$, the value given by Munk and MacDonald for a uniform incompressible fluid. Using a value of 0.82 for $\rho/\bar{\rho}$ gives the observed H_2. This value, along with (7) was used to calculate the geoid anomalies used below. A more complicated two-layer model used to simulate bowing of interior density constants, calibrated on H_2, gives almost identical numerical results, although its functional form is more complicated.

As a result of the requirement that density contrasts be specified to second order, the thermal models used to describe the thermal evolution of the plates should be appropriate for plates which are spherical shells, rather than plane layers. The spherical analogue of the plate model consists of a spherical shell of thickness d which is initially at temperature T_o. At times $t > 0$, the top of the shell (at $r = a$) is held at $T = 0$, while the bottom (at $r = a - d$) is held at T_o.

The temperature at depth z and time t is:

$$T(z,t) = T_o \left\{ \frac{a-d}{a-z} \frac{z}{\ell} + \frac{2a}{(a-z)\pi} \sum \frac{(-1)^{n+1}}{n} \sin \frac{n\pi(d-z)}{d} \exp(-n^2\pi^2\kappa t/d^2) \right\} \quad (9)$$

where κ is thermal diffusivity (20). In the limit $a \to \infty$, this becomes identical to the standard plate model with horizontal conduction of heat neglected (16). The steady-state temperature is less than, while the time-dependent temperature is greater than that for a plane layer plate.

The corresponding expression for the boundary layer model, in which the cooling penetrates arbitrarily deeply into the sphere is:

$$T(z,t) = T_o \left\{ 1 - \frac{a}{a-z} \sum_{n=0}^{\infty} \left[\operatorname{erfc} \frac{[2na+z]}{2\sqrt{\kappa t}} - \operatorname{erfc} \frac{[(2n+2)a+z]}{2\sqrt{\kappa t}} \right] \right\} \quad (10)$$

Only oceanic seafloor less than 200 Myr old is of interest here, so all terms with the exception of the positive, n = 0 term are negligible. Then

$$T = \frac{T_o\, a}{a - z} \left[\operatorname{erf} \frac{z}{2\sqrt{\kappa t}} - \frac{z}{a} \right] \quad (11)$$

The density contrasts leading to geoid anomalies in Eqs. (1) -(6) are

given with respect to some arbitrary reference model. (The undulations of the geoid are insensitive to the details of the reference model). I have taken an old, equilibrium thickness, oceanic plate as the standard for reference (Figure 1). This model has 6.4 km of water (ρ = 1g/cm^3) overlying a 120 km thick plate. The top 6.8 km of the plate is crust with a density of 2.7 g/cm at 0°C; below the crust is mantle of uniform composition. The temperature varies through the plate according to the steady-state part of Equation (9) from 0°C at the top of the crust to T_o at the base of the plate, where the mantle density is taken as 3.3 g/cm^3. Density is related to temperature through a constant coefficient of thermal expansion.

The density structures of the continental crust and lithosphere are not known, although variations can be bounded from observations of the geoid (21). Both vary with location. But since the primary purpose of this paper is to compare models of the oceanic lithosphere, I have arbitrarily adopted a simple uniform continental structure which is in isostatic equilibrium with the reference oceanic model.

Continental lithosphere is assumed to be identical to old oceanic lithosphere. Continental crust is assumed to be 35 km thick and to extend 0.64 km above sea-level. For computational simplicity, its density is assumed constant at 2.7 g/cm^3 in the upper 7.06 km, below which it has a decrease in density paralleling the variation with depth of the density of oceanic crust caused by variation in temperature.

For both the plate model and the boundary layer (sometimes called "cooling half-space") model, the crust is assumed to have

constant thickness. The depth of water is constrained by the requirement that the lithosphere be in isostatic equilibrium with the equilibrium plate reference model. The density profiles for the three-type models are shown schematically in Figure 1.

If equation (7) is rewritten

$$N_{\ell m}(\theta,\phi) = H_\ell n_{\ell m} Y_{\ell m}(\theta,\phi) \quad , \tag{12}$$

then for the spherical analogue of the plate model,

$$n_{\ell m} = \frac{2d^2\, \alpha\, \rho_m T_o G}{\pi^2 g} \frac{\ell}{2\ell+1} \int_{\text{Oceans}} Y_{\ell m}(\theta,\phi) \sum_{n=1}^{\infty} \frac{(-1)^{n+1}}{n^2} \exp(-n^2\pi^2\kappa t/d^2) \sin\theta d\theta d\phi \tag{13}$$

For the boundary layer model,

$$n_{\ell m} = \frac{\alpha \rho_m T_o G}{g} \frac{\ell}{2\ell+1} \int_{\text{Oceans}} \left(\frac{d^2}{6} - \kappa t\right) Y_{\ell m}(\theta,\phi) \sin\theta d\theta d\phi \tag{14}$$

For the continental structure used,

$$n_{\ell m} = 2.67 \cdot 10^{12}\ \text{g/cm}\ \frac{G}{g} \frac{\ell}{2\ell+1} \int_{\text{Continents}} Y_{\ell m}(\theta,\phi) \sin\theta d\theta d\phi \tag{15}$$

In order to evaluate the integrals in (13) - (15), it is necessary to know the age of all oceanic lithosphere as well as that part of the surface which is continental. Mauk (22) compiled the global estimation of seafloor age used in this study on a $5^{\circ} \times 5^{\circ}$ grid. The expansions were carried through degree and order 20.

Model geoids are obtained by summing the terms for each degree and order. Since geoid anomalies are referenced relative to the center of mass of the earth, the degree zero and one terms are not included in the sum.

4. Isostatic Geoid Models

Although the primary purpose of this paper is to compare isostatic geoid anomalies for two models of the thermal structure of oceanic lithosphere, the computed geoids depend upon the model assumed for the subcontinental structure. It is useful to isolate the effect of this structure. Figure 2 shows the geoid calculated using the continental structure in Figure 1 and neglecting the contribution from variation of oceanic lithosphere with age; in this model, all oceanic lithosphere is assumed to have reached thermal equilibrium.

Continental regions in this model are characterized by geoid highs of 5 to 10 meters while oceanic basins show lows of -5 to -10 m. The change in geoid elevation of about 10 m at continental margins matches that observed off the east coast of Australia (23), but is somewhat larger than that seen off the east coast of North American at 40.5°N (8), indicating that the continental structure chosen is perhaps representative, but cannot be applied universally. The geoid anomalies

in the North Atlantic are about 5 m more negative than those in the Pacific. This is a real effect of the three-dimensional nature of the distribution of continents as discussed later, not an artifact of the spherical harmonic expansion.

The model geoid which results when the "observed" variations in lithospheric age are used in the plate model [equation (13)], along with the standard continental model, are shown in Figure 3. Oceanic ridges and continents are characterized by geoid highs of up to 6 m, while geoid lows of about -7 m characterize the regions of Cretaceous seafloor in the Western Pacific, Atlantic, and Indian oceans.

This isostatic geoid is similar to one computed by Chase and McNutt (24) using a spherical harmonic expansion of topography under the assumptions that continental topography is compensated by the Airy mechanism at a depth of 35 km and that oceanic topography (excepting trenches) is compensated at 40 km. The main differences occur locally over high mountains, where their geoid is about 10 m higher than mine, and trenches, where their geoid is about 10 m lower. These differences are to be expected given the differences in the two reference models.

The effect of variation in seafloor age alone, shown in Figure 4, is obtained by subtracting the continental effect (Figure 2) from the combined oceanic age and continental model (Figure 3). The positive contributions from the midoceanic ridges become more obvious. In addition, the contributions to the geoid highs from young lithosphere formed by back-arc spreading in the Western Pacific and off Sumatra become apparent.

Figure 5 is the equivalent of Figure 3, this time calculated

using the spherical boundary layer model of the oceanic lithosphere. It is remarkably similar to Figure 3, with the geoid anomaly over Jurassic oceanic lithosphere differing by only 2 m, almost an order of magnitude less than the 15 m predicted on the basis of the one-dimensional models commonly used (17).

The marked similarity of the model geoids calculated using the full three-dimensional formulation applied to actual lithospheric age distributions is demonstrated directly by calculating the difference between the two models. Figure 6, which shows the difference between the boundary layer model (Fig. 5) and the plate model (Fig. 3), illustrates that the predictions of these two models is never much in excess of ± 2 m. Figure 6 employs a contour interval a factor of 5 smaller than those in the previous models.

5. Discussion

The models usually used in discussing the isostatic geoid (7-9,17) are obtained by assuming 1) that the half-space equation (3) is applicable, and 2) that only local density contrasts (the $k = 0$ wavenumber) is important. This is equivalent to assuming a one-dimensional density model.

The spectra for some of the isostatic geoids shown above are presented in Figure 7. The solid line with solid dots gives the spectrum of the continental geoid (plotted in figure 2). The spectra of the plate plus continent model (Figure 3) and boundary layer plus continent model (Figure 5) are similar to this one. The dashed line with open circles gives the net effect of the young lithosphere in the

plate model. (The geoid for this model was shown in Figure 4.) Both lines show a relative peak at $\ell \approx 4$-5. The spectrum for the difference between the plate and boundary layer models (Fig. 6) shown with crosses, is about a factor of 5 smaller and doesn't reach its relative peak until degree 10. Clearly the one-dimensional geoid models commonly used are inadequate to describe geoid models on a global scale, although they may be useful approximations near ridge-crests and continental margins.

The plate and boundary layer models differ most for seafloor of age 80 My or greater. The largest contiguous area of the seafloor older than 80 My is in the Western Pacific. This region has a diameter of roughly 35° of arc, which accounts for the peak in the spectrum of the difference between the plate and boundary layer isostatic geoid models at $\ell \approx 10$. (The expansion is carried through degree and order 20. Thus, the small difference in predicted geoids is a real effect, not an artifact of truncation of the spherical harmonic expansion). The very small difference between the theoretical geoids for the two thermal models arise because the long wavelength geoid anomalies from ridges and continents common to both models extend into the ocean basins and swamp the short wavelength differences between the models.

The plate-driving force resulting from the thickening of the lithosphere with age is proportional to the integral of the product of the density contrast between the lithosphere and the asthenosphere and depth (25-27). As Parsons and Richter (17) pointed out, using a flat earth model, this driving force is then proportional to the geoid anomaly. Hager and O'Connell (27), using the plate model of the

lithosphere, quantified this driving force on a spherical earth using Mauk's (22) distribution of lithospheric ages. They concluded that it is a significant driving force, distributed over plate area, which can help to explain the observed lack of dependence of oceanic plate velocity on area if plate motion is resisted by basal drag of a few bars. The calculations presented above show that their conclusions would not have changed significantly if they had used the boundary layer model rather than the plate model.

Dahlen (18) advocates using as a definition of isostacy that 1) shear stresses on vertical planes vanish and 2) deviatoric stresses within the isostatically compensated layer be minimized. Requirement 2) leads to an increase in gravitational potential and geoid height by a factor very close to $(\ell + 2)/\ell$ over that used here. I have chosen not to use this definition, preferring the definition used here which leads to a lower gravitational potential of the system. Minimizing deviatoric stress would strengthen the conclusion of this paper, since it amplifies the low-degree harmonics more than the higher ones. It would also lead to a spectrum closer to that of the observed geoid.

It is of interest to compare the isostatic geoids computed here with the observed geoid heights. The top spectrum in Figure 7 is the spectrum of the observed geoid (28). The observed spectrum is redder than the model spectra; at $\ell = 3$ the observed geoid spectrum is a factor of 15 larger than the model ones, although at degree 20 the lithosphere contributes a large amount of power.

Both thermal models of the lithosphere have similar theoretical geoids when the actual distribution of seafloor ages is

used. Stripping the effects of seafloor aging using either model and the uniform continental reference model from the observed geoid should reveal the effects of dynamic processes in the mantle. Figure 8 shows the results of stripping the geoid in Figure 3 from the GEM8 geoid (28). The GEM8 geoid is referred to the hydrostatic figure, (f = 1/299.83), rather than the best-fitting ellipsoid, since any departure from hydrostatic equilibrium must be dynamically supported, and be of geophysical, if not geodetic, interest.

The greatest amplitude anomaly in the stripped geoid remains over West Antarctica, with a value of -120 m. Central Siberia and Hudson Bay have anomalies in excess of -80 m. The low over Ceylon is barely -60 m, and appears to mark the edge of the anomaly stretching over the pole to the eastern U.S. The saddle in the geoid over Tibet is very likely the result of the doubling of crustal thickness there, which would lead to an additional local geoid elevation of about 20 m.

The positions of positive geoid anomalies are not affected much, although there is a small decrease in amplitude over the Western Pacific (back-arc spreading removed) and Africa and S. America, where a small part of the highs are due to the effect of continental crust. Much (about 20 m) of the local geoid high over the Andes is the result of the great thickness there not included in the uniform crustal model.

The main negative features of the residual geoid are two large anomalies; one is centered over W. Antarctica with an amplitude of almost -120 m, the other is larger in area, reaching from Ceylon, through Siberia to Quebec. There are also two large positive anomalies - one over New Guinea, the other centered just west of Africa. It has

been noted that these highs correlate well with subduction and hotspot activity, respectively (29,30). The location of the Mt. Erebus hotspot near the center of the W. Antarctic low, the most pronounced geoidal feature, provides a noted and embarassing exception to the correlation between geoid highs and hotspots.

The magnitude of the observed geoid fluctuation is an order of magnitude larger than those in the model geoids. Nonetheless, recent studies have shown that it is possible to extract the lithospheric signal from the global "noise" in some areas (9,31). In the most comprehensive global study to date, Sandwell and Schubert (31) have shown that the slope of the geoid height vs. age curve can be extracted in several regions. Near ridges these slopes are close to those predicted by one-dimensional models using the plate or boundary layer thermal structures. Further from the ridges the slopes vary and even change signs. Although this type behavior is not predicted by one-dimensional models, inspection of Figures 3 and 6 show 1) that this behavior is to be expected given the three-dimensional nature of the problem, and 2) it cannot be used, given the "noise" in the geoid signal, to discriminate between the plate and boundary layer models.

Although plate and boundary layer models cannot be distinguished using global observations of the geoid, it may still be possible to use geoidal variations across features such as fraction zones to place some constraint on the thermal structure of old lithosphere (32).

Acknowledgements

This paper resulted from discussions with Clive Lister, who pointed out that the earth is round, that topography is three-dimensional, and that one-dimensional, flat earth geoid models are not necessarily applicable. Tony Dahlen pointed out the second order nature of the definition of isostacy and provided a preprint of his paper. This work was supported by the National Aeronautics and Space Administration grant No. NSG-7610. Contribution No. 3577, Division of Geological and Planetary Sciences, California Institute of Technology, Pasadena, California, 91125.

References

1. M. G. Langseth Jr., X. Le Pichon and M. Ewing, Crustal structure of the mid-ocean ridges 5. heat flow through the Atlantic Ocean floor and convection currents, J. Geophys. Res. 71 (1966) 5321-5355.
2. D. L. Turcotte and E. R. Oxburgh, Finite amplitude convective cells and continental drift, J. Fluid Mech. 28 (1967) 29-42.
3. D. P. McKenzie, Some remarks on heat flow and gravity anomalies, J. Geophys. Res. 72 (1967) 6261-6273.
4. J. G. Sclater and J. Francheteau, The implications of terrestrial heat flow observations on current tectonic and geochemical models of the crust and upper mantle of the Earth, Geophys. J. Roy. Astron. Soc. 20 (1970) 509-542.
5. E. E. Davis and C. R. B. Lister, Fundamentals of ridge crest topography, Earth Planet. Sci. Lett. 21 (1974) 405-413.
6. J. G. Sclater, C. Jaupart and D. Galson, The heat flow through oceanic and continental crust and the heat loss of the earth, Rev. Geophys. Space Phys. 18 (1980) 269-311.
7. J. R. Ockendon and D. L. Turcotte, On the gravitational potential and field anomalies due to thin mass layers, Geophys. J. Roy. Astron. Soc. 48 (1977) 479-492.
8. W. F. Haxby and D. L. Turcotte, On isostatic geoid anomalies, J. Geophys. Res. 83 (1978) 5473-5478.
9. W. F. Haxby, The mid-ocean ridge geoid anomaly, EOS, Trans. Am. Geophys. Un. 60 (1979) 391.

10. R. L. Parker and D. W. Oldenburg, Thermal model of ocean ridges, Nature Phys. Sci. 242 (1973) 137-139.

11. E. R. Oxburgh and D. L. Turcotte, Mechanisms of continental drift, Rep. Prog. Phys. 41 (1978) 1249-1312.

12. G. Schubert, D. A. Yuen, C. Froidevaux, L. Fleitout and M. Souriau, Mantle circulation with partial shallow return flow: effects on stresses in oceanic plates and topography of the sea floor, J. Geophys. Res. 83 (1978) 745-758.

13. S. T. Crough, Thermal model of oceanic lithosphere, Nature 256 (1975) 388-390.

14. D. W. Forsyth, The evolution of the uppermantle beneath the mid-ocean ridges, Tectonophysics 38 (1977) 98-118.

15. R. J. O'Connell and B. H. Hager, On the thermal state of the earth in A. Dziewonski and E. Boschi, eds., Physics of the Earth's Interior, Enrico Fermi Internationl School of Physics, Course 78, Soc. Italiana di Fisica, Bologna (1980) 270-317.

16. B. Parsons and J. G. Sclater, An analysis of the variation of ocean floor with age, J. Geophys. Res. 82 (1977) 803-827.

17. B. Parsons and F. M. Richter, A relation between the driving force and geoid anomaly associated with mid-ocean ridges, Earth Planet. Sci. Lett. 51 (1981) 445-450.

18. F. A. Dahlen, A note on isostatic geoid anomalies on a sphere, J. Geophys. Res. (1982) in press.

19. W. H. Munk and G. J. F. MacDonald, The Rotation of the Earth - A Geophysical Discussion, Cambridge Univ. Press, Cambridge (1960).

20. H. S. Carslaw and J. C. Jaeger, Conduction of Heat in Solids, Oxford Univ. Press, Oxford (1959).

21. D. L. Turcotte and D. C. McAdoo, Geoid anomalies and the thickness of the lithosphere, J. Geophys. Res. 84 (1979) 2381-2387.

22. F. J. Mauk, A tectonic-based Rayleigh wave group velocity model for prediction of dispersion character through ocean basins, Ph.D. thesis, University of Michigan, Ann Arbor, Michigan (1977).

23. K. L. Brace, Preliminary Ocean-area geoid from GEOS-III satellite radar altimetry, Defense Mapping Agency, Aerospace Center, St. Louis Air Force Station, Missouri.

24. C. G. Chase and M. K. McNutt, The geoid: effect of compensated topography and uncompensated oceanic trenches, Geophys. Res. Lett. (1982) in press.

25. C. R. B. Lister, Gravitational drive on oceanic plates caused by thermal contraction, Nature 257 (1975) 663-665.

26. B. H. Hager, Oceanic plate motions driven by lithospheric thickening and subducted slabs, Nature 276 (1978) 156-159.

27. B. H. Hager and R. J. O'Connell, A simple global model of plate motions and mantle convection, J. Geophys. Res. 86 (1981) 4843-4867.

28. C. A. Wagner, F. J. Lerch, J. E. Brownd and J. A. Richardson, Improvement in the geopotential derived from satellite and surface data (GEM7 and 8), J. Geophys. Res. 82 (1977) 901-913.

29. C. G. Chase, Subduction, the geoid, and lower mantle convection,

Nature 282 (1979) 464-468.

30. S. T. Crough and D. M. Jurdy, Subducted lithosphere, hotspots, and the geoid, Earth Planet. Sci. Lett. 48 (1980) 15-22.

31. D. Sandwell and G. Schubert, Geoid height versus age for symmetric spreading ridges, J. Geophys. Res. 85 (1980) 7235-7240.

32. D. Sandwell, written communication (1981).

Figure Captions

Figure 1. Density models used in calculating isostatic geoid anomalies. A mature oceanic plate 120 km thick (right center and dashed lines) is taken as a reference model. Continental structure (far right) is assumed uniform; the subcontinental lithosphere is assumed to be equivalent to old oceanic lithophere. Near the ridge (left center) the plate and boundary layer models are equivalent. For old lithosphere, cooling penetrates deeper into the mantle for the boundary layer model (far left) than for the plate model. The increased thickness of the lithosphere is compensated by additional subsidence.

Figure 2. Model isostatic geoid resulting from the contrast in density structures between continents and oceans. The effects of oceanic age variation are not included; all oceanic lithosphere is assumed to be mature plate in thermal steady state. The contour interval is 5 m.

Figure 3. Isostatic geoid resulting from the variation in thermal structure with age of the plate model and from the contrast in density structure between continents and oceans.

Figure 4. Isostatic geoid resulting from only the variation in thermal structure with age for the plate model. This figure represents the difference between the geoids in Figure 3 and

Figure 2.

Figure 5. Isostatic geoid resulting from the variation in thermal structure with age of the boundary layer model and from continents.

Figure 6. Difference in isostatic geoids for the boundary layer and plate models, obtained by subtracting the geoid in Figure 3 from that in Figure 5. The contour interval is only 1 m. If one-dimensional models were applicable, the maximum difference would be 15 m.

Figure 7. Spectra for different geoids. The top line is the observed nonhydrostatic geoid. The solid line with solid dots shows the effect of continental structure alone. The dashed line with open circles is the spectrum of the contribution of variations in oceanic age assuming the plate model. The bottom line represents the spectrum of the difference between the geoids of the boundary layer and plate models.

Figure 8. Residual geoid through degree and order 20 obtained by subtractng the isostatic geoid in Figure 3 from the GEM8 geoid referred to the hydrostatic flattening (f = 1/299.83).

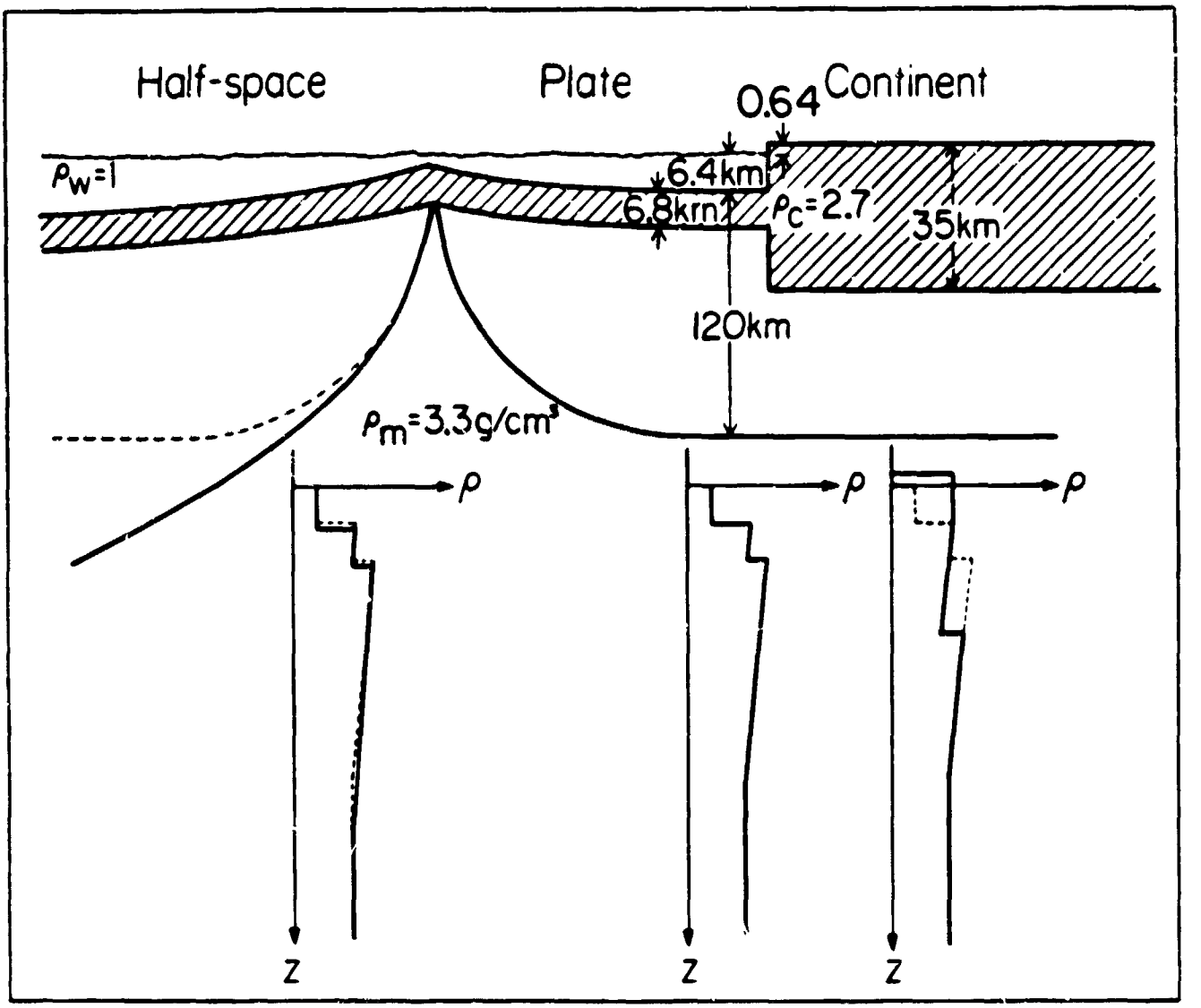
Half-space
Plate
0.64
Continent
ρ_w=1
6.4km
6.8krn
ρ_c=2.7
35km
120km
ρ_m=3.3g/cm³
ρ
ρ
ρ
Z
Z
Z

Fig. 1

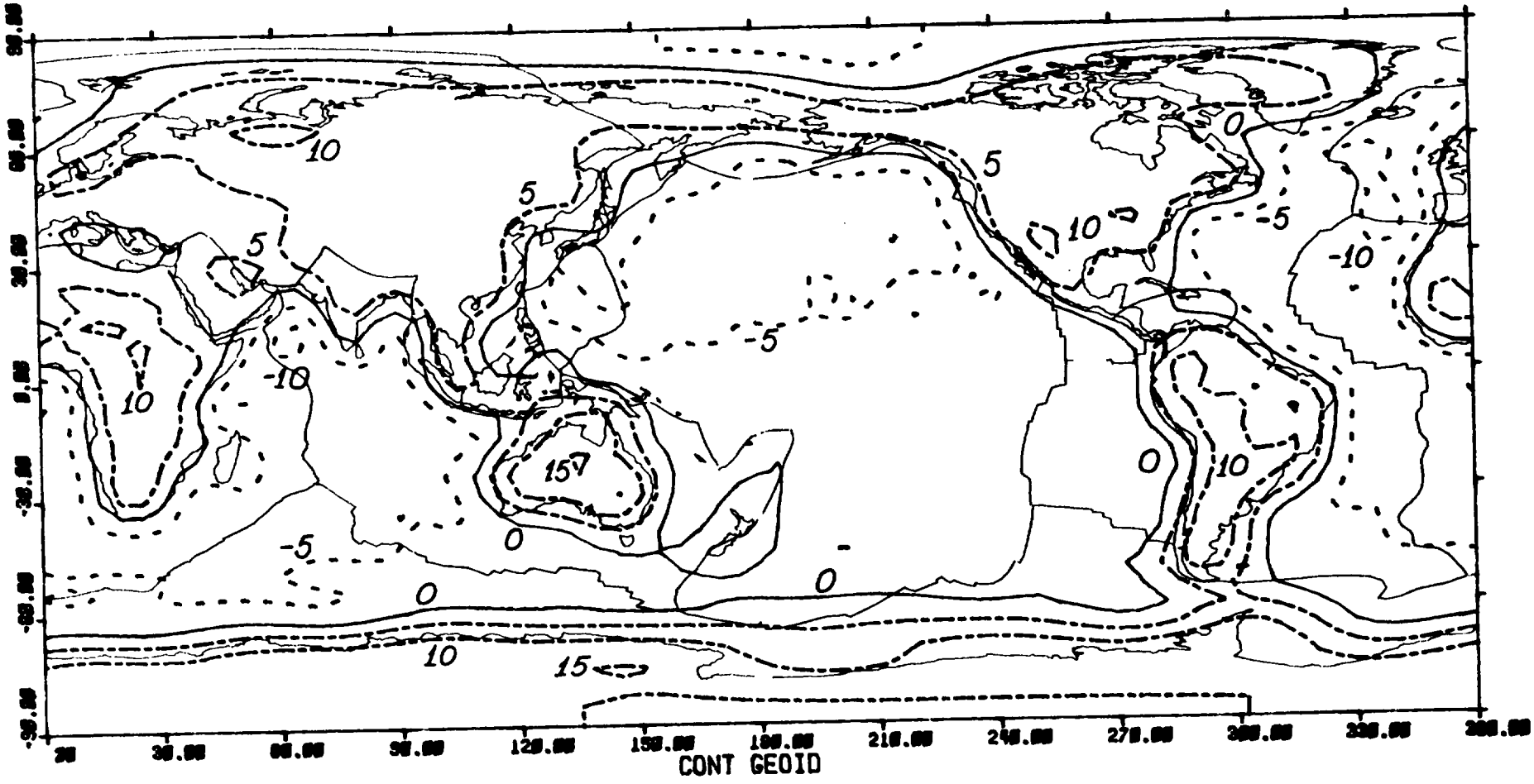

Fig. 2

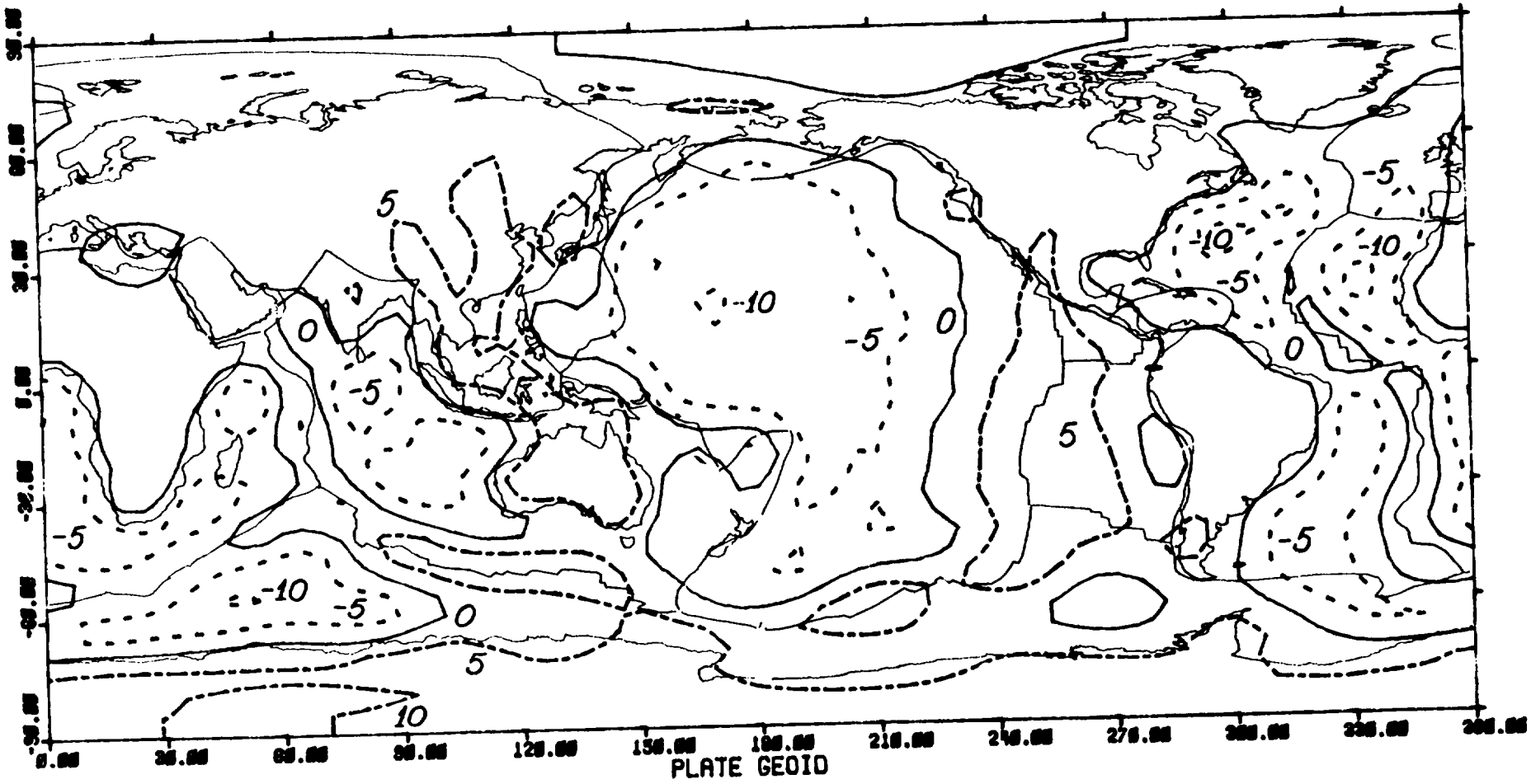

Fig. 3

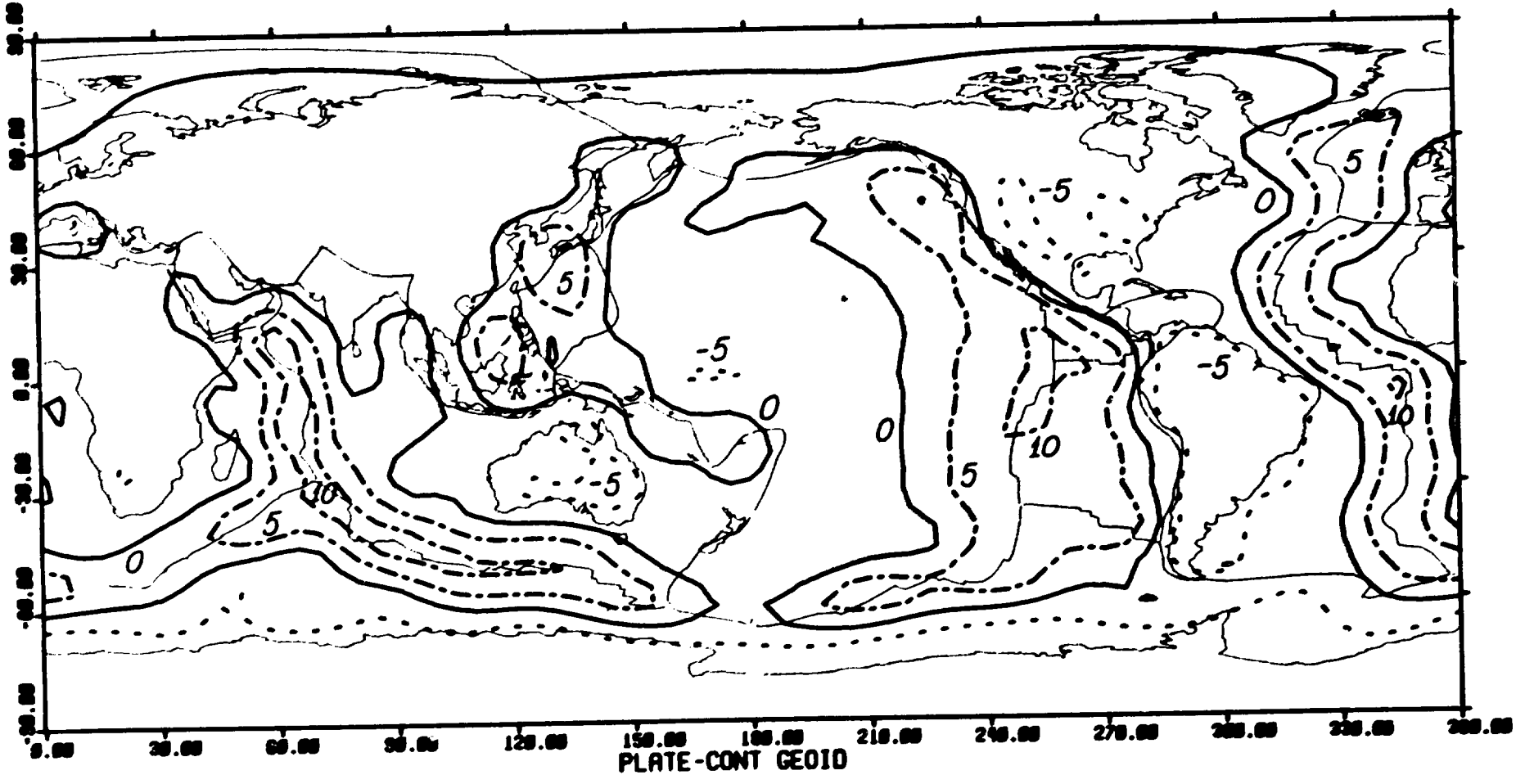

Fig. 4

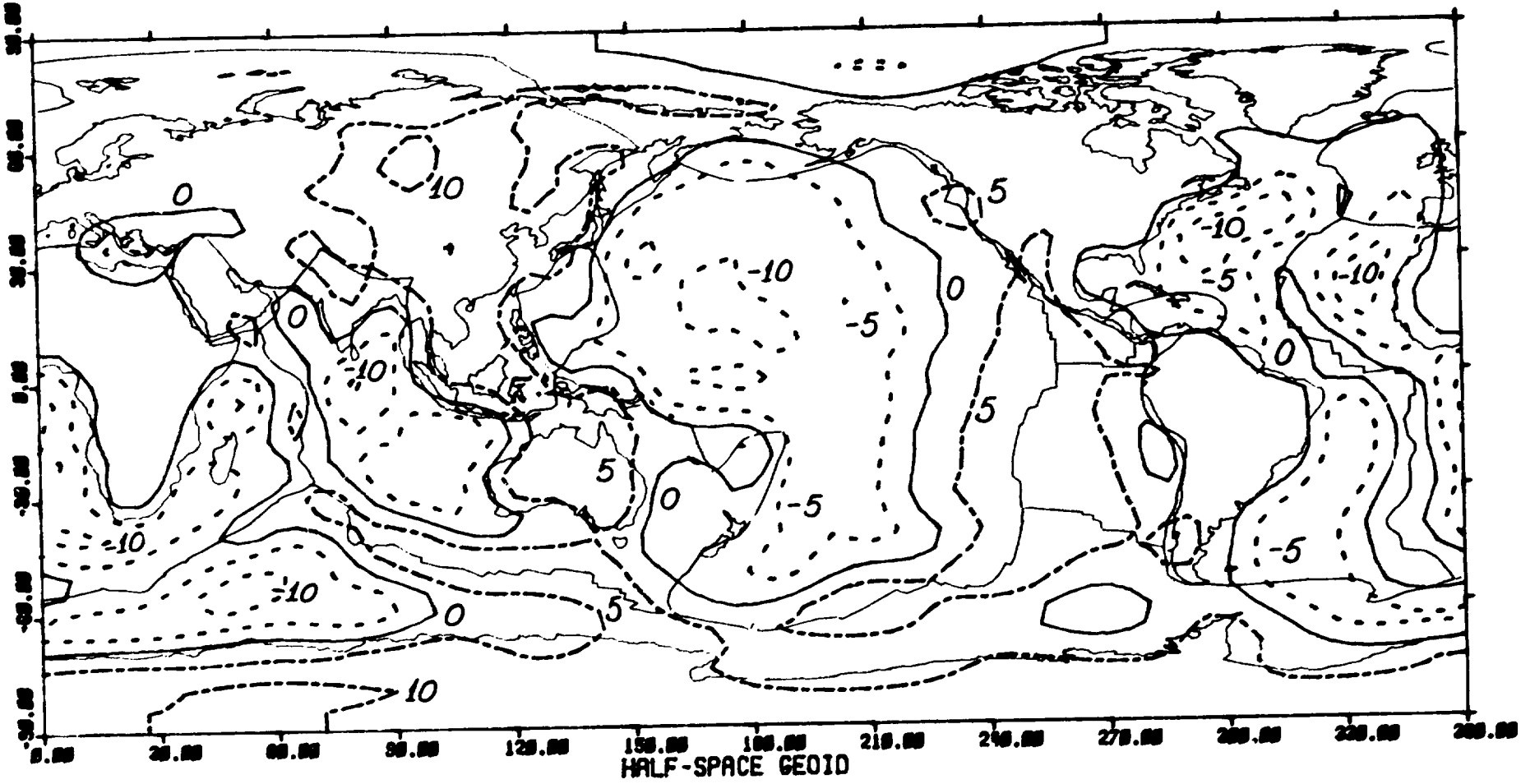

Fig. 5

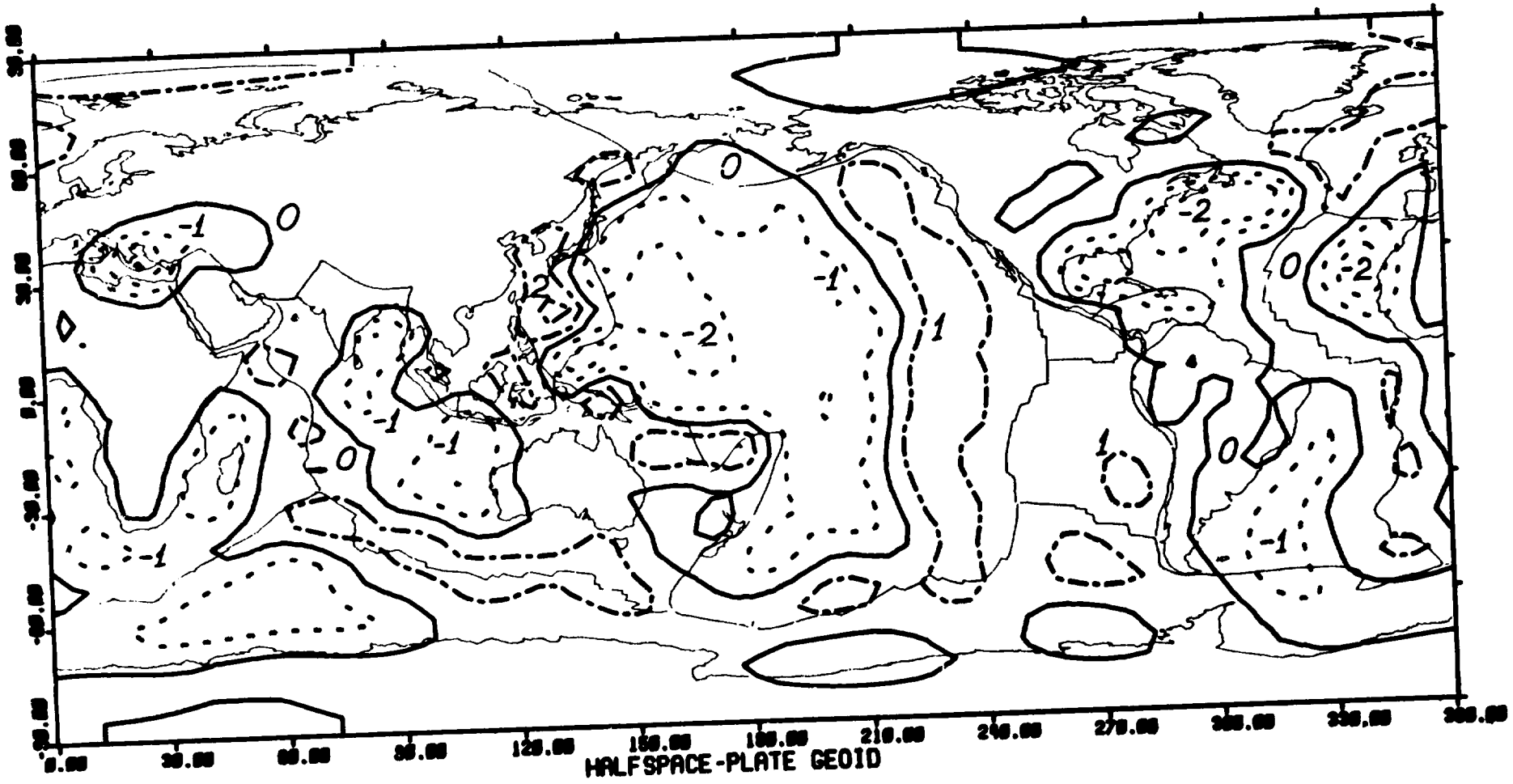

Fig. 6

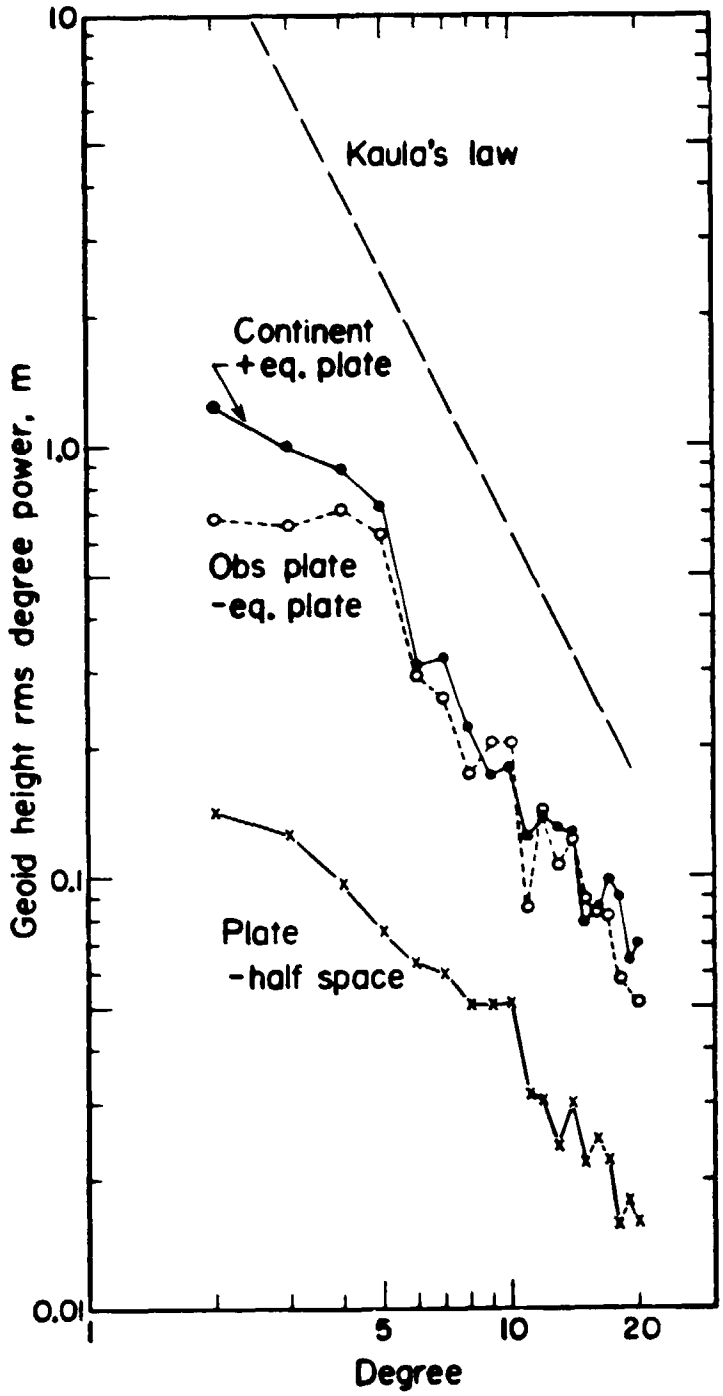
10
1.0
0.1
0.01
Geoid height rms degree power, m
Kaula's law
Continent
+eq. plate
Obs plate
-eq. plate
Plate
-half space
1
5
10
20
Degree

Fig. 7

ORIGINAL PAGE IS
OF POOR QUALITY

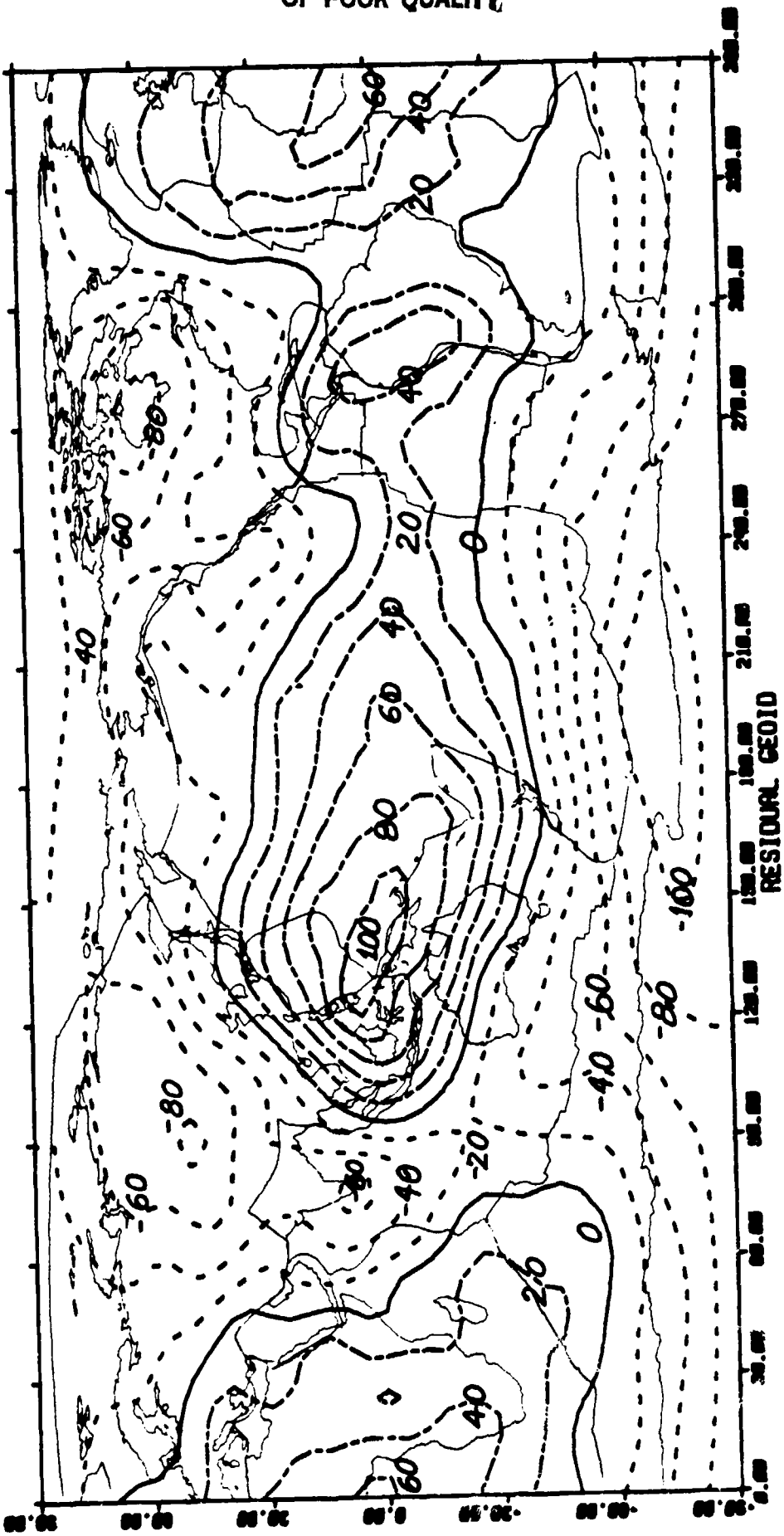

Fig. 8